JOURNAL OF GEOPHYSICAL RESEARCH, VOL. 113, B06204, doi:10.1029/2007JB005275, 2008

Pressure-volume-temperature relations in MgO: An ultrahigh pressure-temperature scale for planetary sciences applications

Zhongqing Wu,[1] Renata M. Wentzcovitch,[1] Koichiro Umemoto,[1] Baosheng Li,[2] Kei Hirose,[3] and Jin-Cheng Zheng[4]

Received 18 July 2007; revised 18 January 2008; accepted 10 March 2008; published 20 June 2008.

[1] In situ crystallography based on diamond anvil cells have been extended to the multimegabar regime. Temperatures in these experiments have crossed the 2500 K mark. Yet, current high pressure-temperature (*PT*) standards of calibration produce uncertainties that inhibit clear conclusions about phenomena of importance to planetary processes, e.g., the postperovskite transition in Earth's mantle. We introduce a new thermal equation of state (EOS) of MgO which appears to be predictive up to the multimegabar and thousands of kelvin range. It is obtained by combining first principles local density approximation quasi-harmonic (QHA) calculations with experimental low-pressure data. This EOS agrees exceptionally well with shock compression data. The postspinel and postperovskite phase boundaries recalculated using our EOS match seismic observations. The latter, in particular, supports the idea that postperovskite transforms back to perovskite before the core-mantle boundary. The recalculated experimental Clapeyron slope of the postperovskite transition is also more consistent with those obtained by first principles calculations.

Citation: Wu, Z., R. M. Wentzcovitch, K. Umemoto, B. Li, K. Hirose, and J.-C. Zheng (2008), Pressure-volume-temperature relations in MgO: An ultrahigh pressure-temperature scale for planetary sciences applications, *J. Geophys. Res.*, *113*, B06204, doi:10.1029/2007JB005275.

1. Introduction

[2] Diamond anvil cell studies have revealed several properties of materials at extreme pressures and temperatures (*PT*) [*Murakami et al.*, 2004; *Loubeyre et al.*, 2002; *Isshiki et al.*, 2004; *Dubrovinsky et al.*, 2003] that are important for understanding planetary interiors. The significance of these observations depends critically on the precise measurement of pressure using a reliable standard. In previous high-pressure experiments, the EOSs of metals such as Au and Pt and nonmetals like MgO and NaCl have been commonly used as standards. Unfortunately, discrepancies have been observed when different standards or the same standard but different EOSs are used. The discrepancy in pressure becomes larger at high temperatures, resulting in uncertainties as large as 4 GPa at 2200 K [*Fei et al.*, 2004a]. For example, the postspinel transformation pressure in olivine is found to be significantly lower than that of the 660 km seismic discontinuity by more than 2 GPa if the Au scale of *Anderson et al.* [1989] is used. In contrast, if the MgO pressure scale of *Speziale et al.* [2001] is used, the transformation boundary is close to the 660 km seismic discontinuity. The large discrepancy observed in these studies could lead to different understanding of the nature of the 660 km seismic discontinuity and therefore of the mantle dynamics. The discrepancy in pressure is more significant at pressures over 100 GPa. The simultaneous X-ray diffraction measurements of the volumes of Au and Pt, for example, showed that the Pt pressure scale, i.e., its EOS, predicts pressures higher than Au by about 15 GPa at ~120 GPa, even at room temperature [*Akahama et al.*, 2002; *Dewaele et al.*, 2004]. These discrepancies have prompted studies to build internally consistent pressure scales [*Fei et al.*, 2007; *Dorogokupets and Oganov*, 2007].

[3] The EOSs of MgO have been extensively investigated by several semiempirical, simplified nonempirical models [*Zhang and Bukowinski*, 1991; *Inbar and Cohen*, 1995; *Matsui et al.*, 2000], and first principles calculations [*Karki et al.*, 1999, 2000; *Oganov and Dorogokupets*, 2003a; *Lu et al.*, 2005; *Alfè et al.*, 2005]. Among these studies, the thermodynamic properties of MgO at high *PT*s have been best described by first principles quasi-harmonic (QHA) calculations [*Karki et al.*, 1999, 2000; *Oganov and Dorogokupets*, 2003; see also *Alfè et al.*, 2005] within the regime of validity of this approximation [*Wentzcovitch et al.*, 2004]. This means that thermal pressure in first principle QHA calculations is considerably precise, which is very helpful since the experiments suffer from large uncertainties

[1]Department of Chemical Engineering and Materials Science and Minnesota Supercomputing Institute, University of Minnesota Twin Cities, Minneapolis, Minnesota, USA.
[2]Mineral Physics Institute, State University of New York at Stony Brook, Stony Brook, New York, USA.
[3]Department of Earth and Planetary Sciences, Tokyo Institute of Technology, Tokyo, Japan.
[4]Condensed Matter Physics and Materials Science Department, Brookhaven National Laboratory, Upton, New York, USA.

0148-0227/08/2007JB005275$09.00

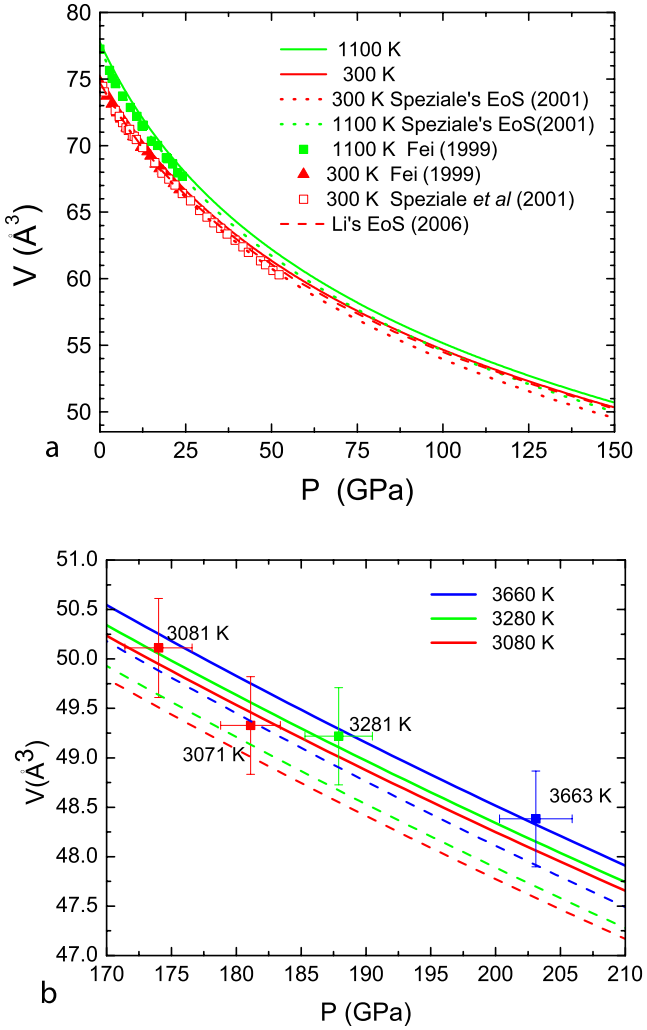

Figure 1. Comparison between our uncorrected EOS with (a) quasi-static compressive results at 300 K and 1100 K and (b) shock wave data [*Svendsen and Ahrens*, 1987]. Dashed line is *Speziale et al.*'s [2001] EOS.

in the thermal pressure. At very high temperatures, e.g., above ~1000 K at ambient pressure, anharmonic effects are nonnegligible and must be accounted for. We present here first principles high-temperature QHA calculations of MgO, which are in exceptional agreement with high *PT* shock wave data. Our calculated EOS also agrees well with the *Li et al.*'s [2006] absolute pressure scale. Therefore, our EOS can be directly used as pressure scale at ultrahigh pressures. At low pressures, we combine our results with experimental data to correct for insufficiencies of our first principles treatment (small volume overestimation of ~0.6%). We also introduced a semiempirical anharmonic correction that expands the temperature range of application of our earlier EOS based on the QHA.

2. Method

[4] Computations were performed using density functional theory within the local density approximation (LDA) [*Ceperley and Alder*, 1980; *Perdew and Zunger*, 1981]. The magnesium pseudopotential was generated by the method of U. von Barth and R. Car (unpublished method, 1992) (for a brief description of this method, see *Dal Corso et al.* [1993]). Five configurations $3s^2 3p^0$, $3s^1 3p^1$, $3s^1 3p^0 0.53d^0 0.5$, $3s^1 3p^0 0.5$, $3s^1 3d^1$ with decreasing weights 1.5, 0.6, 0.3, 0.3, and 0.2, respectively, were used. Cutoff radii are $r(3s) = r(3p) = r(3d) = 2.5au$, with d locality. The oxygen pseudopotential was generated by the method of *Troullier and Martins* [1991] with the configuration $2s^2 2p^4$. Cutoff radii are $r(2s) = r(2p) = 1.45au$, with p locality. The plane wave energy cutoff is 90 Ry. The Brillouin zone sampling for electronic states was carried out on a 4 × 4 × 4 k mesh with a shift of (1/2, 1/2, 1/2) for both, the NaCl-type and CsCl-type structures. Static pressures at 76.44 Å^3 using a 4 × 4 × 4 k mesh (10 k points) and a 6 × 6 × 6 k mesh (28 k points) differ by less than 0.01 GPa. Dynamical matrices were computed on a 4 × 4 × 4 q mesh using density functional perturbation theory [*Baroni et al.*, 2001] and then interpolated in a 16 × 16 × 16 q mesh to produce the vibrational density of states. Although the 12 × 12 × 12 q mesh for interpolations is sufficient, we adopted a 16 × 16 × 16 q mesh in this work. The pressure difference between 16 × 16 × 16 and 12 × 12 × 12 q mesh is at most 0.05 GPa at 3000 K and 0 GPa. Thermodynamic properties were determined using the quasi-harmonic approximation (QHA) [*Wallace*, 1972]. Within this approximation, the Helmholtz free energy is given by

$$F(V,T) = U_0(V) + \frac{1}{2}\sum_{q,j}\hbar\omega_j(q,V) + k_B T \sum_{q,j}\ln\left\{1 - \exp\left[-\hbar\omega_j(q,V)/k_B T\right]\right\} \quad (1)$$

where the first, second, and third terms are the internal, zero point, and vibrational contributions, respectively. The calculated Helmholtz free energy versus volume was fitted to isothermal fourth-order finite strain equations of state (EOSs). The corresponding P versus V were described by a fourth-order Birch-Murnaghan EOS,

$$P = \frac{3}{2}K_0\left[(V_0/V)^{7/3} - (V_0/V)^{5/3}\right]\left\{1 + \frac{3}{4}(K_0' - 4)\left[(V_0/V)^{2/3} - 1\right] + \frac{3}{8}\left[K_0 K_0'' + (K_0' - 3)(K_0' - 4) + 35/9\right]\left[(V_0/V)^{2/3} - 1\right]^2\right\} \quad (2)$$

where V_0 is volume at zero pressure, K_0 is bulk modulus, $K_0' = (dK/dP)_{P=0}$, and $K_0'' = (d^2K/dP^2)_{P=0}$.

3. Equation of State

[5] Our first principles compression curves at t = 300 K and t = 1100 K are shown in Figure 1a. Our EOS parameters at room temperature are listed in Table 1 and compared with experimental data and other calculations. Our calculated volume, bulk modulus, and its pressure derivative agree well with experimental results. Our equilibrium volume differs from the experimental one by less than 0.6% at

Table 1. Equation of State Parameters for MgO[a]

V_0 (Å^3)	K_0 (GPa)	K_0'	K_0'' (GPa^{-1})	Source
		Experiments		
74.74	161.4	4.29		*Vassiliou and Ahrens* [1981]
74.7	160.2	4.15		*Jackson and Neisler* [1982]
74.71	153	4.1		*Utsumi et al.* [1998]
74.78	160	4.15		*Fei* [1999]
74.71	161	3.94		*Dewaele et al.* [2000]
74.71	160.2	3.99		*Speziale et al.* [2001]
74.71	160.2	4.03		*Zha et al.* [2000][b]
74.7	161.3	4.24		*Li et al.* [2006][b]
		Calculations		
75.19	160	4.23	−0.0281	This study (uncorrected LDA + PP)
75.11	163.2	4.11		This study (uncorrected LDA +PP)
76.2	172	4.004	−0.025	*Oganov et al.* [2003] (LDA+PP)
74.71	160.31	4.18		*Dorogokupets and Oganov* [2007](semiempirical)
74.49	160.5	4.1		*Matsui et al.* [2000] MD simulation
68.82	183	−4		*Alfè et al.* [2005] QMC static
73.9	171.3	4.09		This study (uncorrected LDA+PP static)
72.1	173.2	4.09		This study (uncorrected LDA+LAPW static)
72.4	172	4.09		*Mehl et al.* [1988] (LDA+LAPW static)
77.629	151.707	4.212		*Oganov et al.* [2003](GGA+PP static)
76.049	154.183	4.141		*Oganov et al.* [2003](GGA+PAW static)

[a]All results are at room temperature and zero pressure except those denoted by static. LDA, local density approximation; GGA, generalized gradient approximation; PP, pseudopotential; LAPW, linearized augmented plane wave; APW, projector augmented-wave method; MD, molecular dynamic; QMC, quantum Monte Carlo.
[b]Absolute pressure measurement.

ambient conditions. Although small this difference can produce a 1 GPa pressure difference if the genuine theoretical result is used as pressure calibrant (see Figure 1a). With increasing pressure, the electronic system can be better described by the theory of the inhomogeneous electron gas at the LDA level. Differences between calculated and experimental volumes are then expected to decrease with pressure. Indeed, our EOSs agree exceptionally well with shock wave data [*Svendsen and Ahrens*, 1987] (Figure 1b). One of the important contributions of first principles calculations to the development of EOSs is the computation of thermal effects. The thermal pressure can be calculated quite precisely. Thermodynamic properties, in general, can be obtained quite accurately within the regime of validity of the QHA, and MgO showcases this [*Karki et al.*, 1999, 2000]. This is also displayed in both, Figures 1a and 1b. The exceptional agreement between the direct first principles EOS and shock wave data imply that these results can be directly used for pressure calibration at ultrahigh pressures such as P > 100 GPa. This statement is also supported by the agreement between *Li et al.*'s [2006] absolute pressure EOS, whose parameters are measured directly hence avoiding using pressure standard, and our first principles results. The pressure difference between our and Li et al.'s EOS is only 1.2 (0.5) GPa at 100 (200) GPa (Figure 1a).

[6] Table 2 shows the isochors of MgO obtained directly from our first principles calculations. One sees that the thermal pressure, P_T, varies approximately linearly with temperature and is nearly insensitive to volume. P_T (2000 K) − P_T (300 K) is ∼11 GPa at V/V_o = 1.0 or at 0.625. This is consistent with *Anderson*'s [1997] results and other calculations [*Karki*, 2000; *Oganov and Dorogokupets*, 2003a]. One can also see that the calculated pressure is 1.02 GPa at experimental ambient conditions. Therefore some kind of correction is needed for our EOS to be predictive with the same experimental accuracy at low pressures. Since such correction must vanish at high P, we choose the simple form

$$\Delta V = \Delta V_0 \exp(-P/P_c) \tag{3}$$

ΔV_0 is the difference between our calculated and experimental zero pressure equilibrium volumes. We change V by ΔV in P versus V curves. This correction has negligible effect on the thermal pressure since it is independent of temperature and thermal pressure is insensitive to volume, as pointed above. This type of correction in volume is more satisfactory than the usual "pressure shift," at least in the case of MgO. P_c is a parameter that remains to be determined and we do so by comparing our EOS with experimental data on MgO at low pressures.

[7] In order to determine P_c one must carefully select the data. In quasi-hydrostatic compressive experiments, pressure is determined by internal pressure calibrants. The EOSs derived from these experiments inevitably inherit the uncertainties of these pressure scales [*Fei et al.*, 2004a]. In order to avoid this problem, *Ruoff et al.* [1973] proposed a method to determine absolute pressures by simultaneous measurements of density and elasticity. This measurement had been limited to very low pressures, but more recently *Li et al.* [2006] and *Zha et al.* [2000] extended it to higher pressures. In these experiments, EOS parameters, i.e., V_0, K_0 and K_0', are obtained directly and pressure can then be obtained using the third-order Birch-Murnaghan EOS. These absolute pressure data, together with quasi-hydrostatic compression data at low pressures, and shock wave data have been used to determine P_c. The results after volume correction with P_c = 80 GPa are in extremely good agreement with

Table 2. Isochores for MgO[a]

x = V/V$_o$	300 K	1000 K	2000 K	3000 K	4000 K	5000 K
1.000	1.03	5.35	12.02	*18.74*	*25.49*	*32.24*
	(0.00)	(4.24)	(10.68)	*(17.10)*	*(23.49)*	*(29.84)*
0.975	5.42	9.72	16.40	*23.14*	*29.91*	*36.68*
	(4.31)	(8.54)	(15.01)	*(21.46)*	*(27.88)*	*(34.28)*
0.950	10.42	14.70	21.39	*28.15*	*34.94*	*41.73*
	(9.23)	(13.45)	(19.94)	*(26.43)*	*(32.89)*	*(39.32)*
0.925	16.13	20.38	27.08	*33.86*	*40.67*	*47.48*
	(14.86)	(19.06)	(25.58)	*(32.11)*	*(38.61)*	*(45.08)*
0.900	22.64	26.87	33.58	*40.39*	*47.21*	*54.05*
	(21.31)	(25.49)	(32.04)	*(38.60)*	*(45.14)*	*(51.65)*
0.875	30.09	34.29	41.02	47.84	*54.69*	*61.55*
	(28.70)	(32.85)	(39.43)	(46.04)	*(52.62)*	*(59.18)*
0.850	38.62	42.79	49.53	56.38	*63.26*	*70.15*
	(37.19)	(41.31)	(47.92)	(54.57)	*(61.20)*	*(67.81)*
0.825	48.41	52.54	59.30	66.18	*73.10*	*80.02*
	(46.95)	(51.05)	(57.69)	(64.39)	*(71.07)*	*(77.73)*
0.800	59.66	63.75	70.54	77.46	*84.41*	*91.38*
	(58.20)	(62.26)	(68.94)	(75.69)	*(82.44)*	*(89.16)*
0.775	72.61	76.68	83.49	90.46	97.46	*104.48*
	(71.18)	(75.22)	(81.94)	(88.75)	(95.56)	*(102.35)*
0.750	87.58	91.60	98.46	105.48	112.55	*119.63*
	(86.20)	(90.21)	(96.98)	(103.86)	(110.75)	*(117.63)*
0.725	104.90	108.90	115.81	122.90	130.03	*137.19*
	(103.62)	(107.59)	(114.42)	(121.39)	(128.37)	*(135.34)*
0.700	125.02	128.99	135.96	143.14	150.36	157.61
	(123.86)	(127.81)	(134.71)	(141.78)	(148.87)	(155.94)
0.675	148.46	152.40	159.46	166.73	174.07	181.43
	(147.46)	(151.38)	(158.37)	(165.55)	(172.76)	(179.97)
0.650	175.88	179.79	186.94	194.34	201.80	209.30
	(175.04)	(178.94)	(186.03)	(193.35)	(200.70)	(208.06)
0.625	208.06	211.95	219.21	226.75	234.37	242.01
	(207.40)	(211.28)	(218.49)	(225.96)	(233.47)	(241.00)
0.600	245.99	249.87	257.26	264.96	272.74	280.56
	(245.51)	(249.37)	(256.72)	(264.35)	(272.05)	(279.76)
0.575	290.92	294.78	302.30	310.17	318.14	326.15
	(290.59)	(294.44)	(301.92)	(309.73)	(317.62)	(325.53)
0.550	344.41	348.22	355.87	363.92	372.07	380.27
	(344.21)	(348.01)	(355.62)	(363.61)	(371.69)	(379.79)
0.525	408.43	412.17	419.90	428.09	436.40	444.77
	(408.32)	(412.05)	(419.74)	(427.88)	(436.11)	(444.37)
0.500	485.51	489.11	496.84	505.09	513.48	521.93
	(485.46)	(489.05)	(496.74)	(504.93)	(513.23)	(521.58)

[a]Our direct first principles results are given. Values in parentheses show results after correction with Pc = 80 GPa and c = 0.1 (see text). The experimental equilibrium volume is V_o = 74.71 Å^3. Values in italics are outside the region of validity of our EOS.

pressure data from *Zha et al.* [2000] and *Li et al.* [2006] in the pressure range of 0–11 GPa (Figure 2a), with pressure differences being less than 0.1 GPa at 10 GPa. The results also agree well with quasi-hydrostatic compression data in the range 0–20 GPa (Figure 2b) and with *Li et al.* [2006] data up to and beyond 150 GPa (Figure 2a). This correction with P_c = 80 GPa affects very little results at shock *PT*s, e.g., pressure decreases by ~0.4 GPa at 250 GPa and 300 K. Changing P_c from 50 GPa to 100 GPa has very small effect on pressures (at most 1 GPa at 100 GPa).

[8] Figure 3a shows the EOS at 300 K and 1100 K after the volume correction (P_c = 80 GPa). Our EOS agrees extremely well also with high-temperature data. At 1100 K, V_0 = 77.26 Å^3, which is very similar to the experimental one, 77.24 Å^3. The consistency is not surprising because the QHA is expected to work well up to ~1100 K. Our calculated thermodynamics properties are in excellent agreement with experimental results [see *Karki et al.*, 2000] within the range of validity of the QHA, which is defined by the position of the inflection point in the thermal expansivity versus temperature curve at high temperatures [*Wentzcovitch et al.*, 2004; *Carrier et al.*, 2007]. Beyond the QHA validity limit, intrinsic anharmonic effects arising from phonon-phonon interactions become nonnegligible [*Karki et al.*, 1999, 2000; *Wentzcovitch et al.*, 2004], especially at low pressures.

[9] Here we adopt a simple semiempirical correction (Z. Wu and R. M. Wentzcovitch, A simple semi-empirical anharmonic correction to the quasi-harmonic approximation, manuscript in preparation, 2007) to QHA results to account for intrinsic anharmonic effects. Behind this type of correction there is one essential idea: the assumption that even in the presence of anharmonic effects the QHA free energy expression (equation (1)) is still applicable if

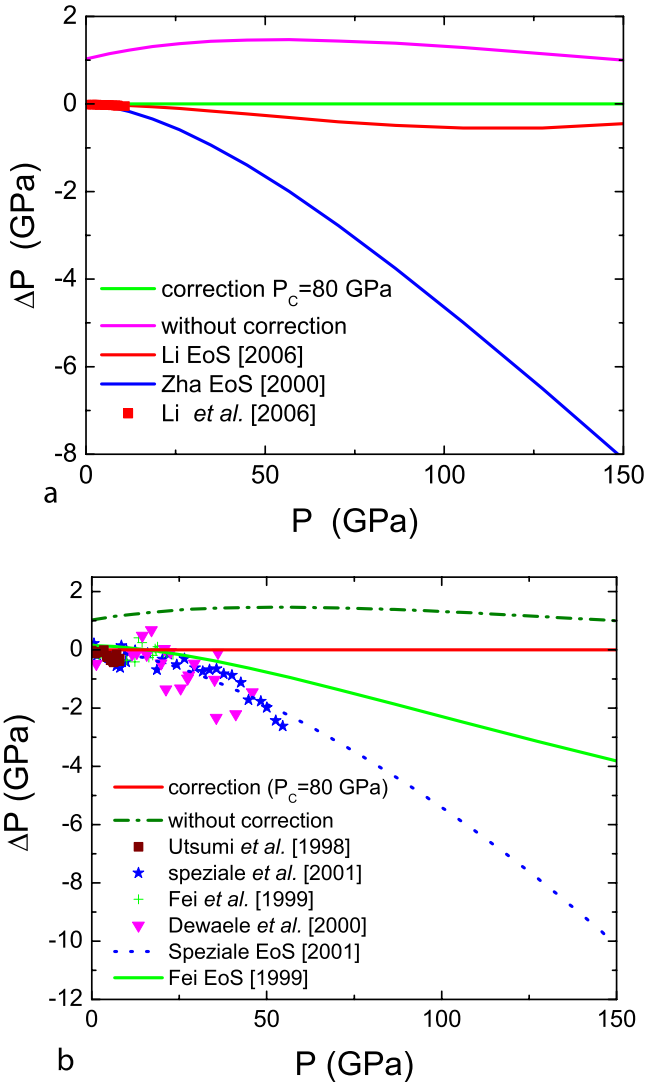

Figure 2. Difference in pressure between other scales and our first principles results (LDA+QHA) corrected by equation (3) only (anharmonic effect at room temperature is negligible). Comparison with (a) absolute scales from *Li et al.* [2006] EOS and *Zha et al.* [2000] EOS and (b) quasi-hydrostatic data.

somehow it is possible to adopt "temperature renormalized" phonon frequencies [*Wallace*, 1972]. In a material like MgO, which has no phonon softening in the *PT* regime of our investigation, it is plausible to assume that at constant volume, phonon frequencies may increase with temperature. We capture this temperature dependence by relating the "renormalized frequencies" at high T with the calculated quasi-harmonic frequencies at a different volume:

$$\Omega(V,T) = \omega(V') \neq \omega(V) \tag{4}$$

where $\Omega(V, T)$ is the "renormalized frequency" at $V - T$, $\omega(V)$ is the T-independent frequency at V, and $\omega(V')$ is the same at V'. Because anharmonic effects become more prominent at high temperatures and less pronounced at high pressures, we choose the following expression for V':

$$V' = V(P,T)\{1 - c^*[V(P,T) - V(P,0)]/V(P,0)\} \tag{5}$$

where c is a constant parameter to be empirically determined. Then we have

$$\begin{aligned} F_c(V,T) &= U_0(V) + \frac{1}{2}\sum_{q,j}\hbar\omega_j(q,V') \\ &\quad + k_BT\sum_{q,j}\ln\{1 - \exp[-\hbar\omega_j(q,V')/k_BT]\} \\ &= U_0(V) - U_0(V') + F_0(V',T) \end{aligned} \tag{6}$$

where F_0 and F_c are the standard QHA (equation (1)) free energy and the modified free energy, respectively, that accounts for anharmonic effects. This correction introduces only one adjustable parameter, c. As shown in Figure 3b and results from Z. Wu and R. M. Wentzcovitch (manuscript in preparation, 2007), anharmonic effects on thermodynamics properties can be satisfactorily captured in this way by choosing an appropriate value for this parameter, in this case c = 0.1. For instance, volumes and other thermodynamic quantities (Z. Wu and R. M. Wentzcovitch, manuscript in preparation, 2007) are still in excellent agreement with the experimental data even at T∼3000 K (Figure 3b). The Grüneisen parameter, shown in Figure 3, also agrees much better with experimental values of *Isaak et al.* [1989] after the anharmonic correction. Figure 3c compares values with c = 0.0, i.e., QHA, c = 0.1, the optimized value for MgO, experimental results, and results by *Oganov and Dorogokupets* [2003]. This semiempirical approach expands considerably the temperature range of validity of our EOS with respect to that obtained by the standard QHA [*Karki et al.*, 2000] (see Figure 4).

[10] MgO is an ideal ultrahigh pressure standard not only because it has a simple structure but also because it is very stable against pressure. No phase transition has been

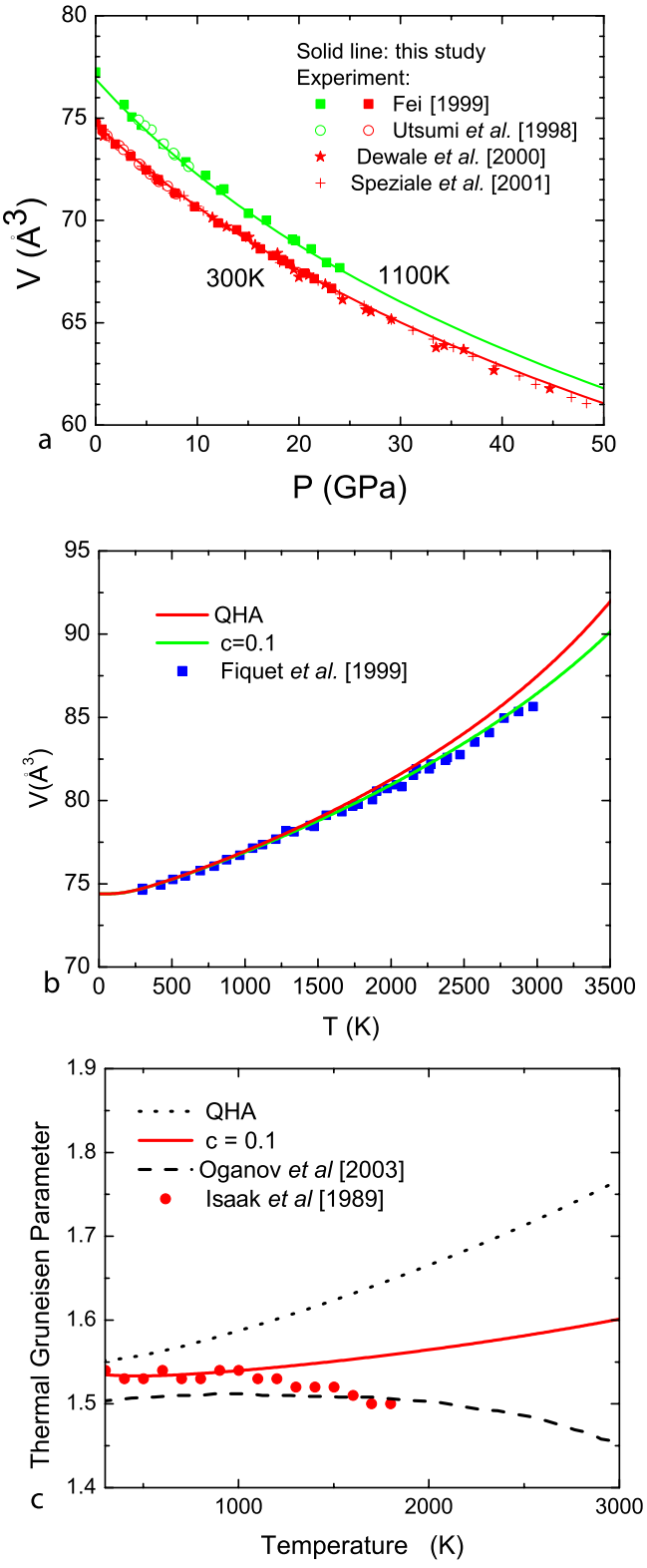

Figure 3. (a) Equation of states at 300 K and 1100 K after volume (P_c = 80 GPa in equation (3)) and anharmonic (c = 0.1 in equation (6)) corrections to the QHA results. (b)Volume versus temperature at ambient pressure based on the volume corrected (equation (3)) EOS with and without anharmonic (equation (6)) correction compared with experimental data by *Fiquet et al.* [1999]. (c) Grüneisen parameters with and without anharmonic (equation (6)) correction compared with experimental data by *Isaak et al.* [1989] and calculated results with anharmonic correction by *Oganov et al.* [2003].

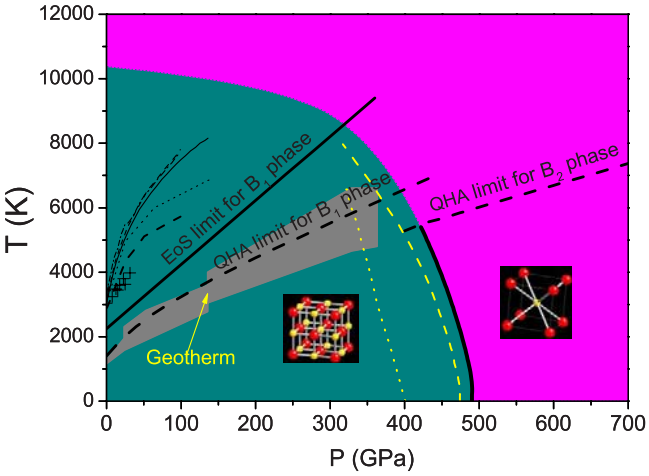

Figure 4. Phase diagram of MgO. The upper limit of validity of our EOS is marked by the black solid line. For comparison, we also show the QHA limit for both phases (marked by dashed lines). The experimental melting curves are from *Zerr and Boehler* [1994] (cross). Theoretical melting curves are from *Alfè* [2005] (solid line), *Belonoshko and Dubrovinsky* [1996] (heavy dashed line), *Strachan et al.* [1999] (dotted line), *Cohen and Gong* [1994] (dashed line), and *Vočadlo and Price* [1996] (dash dotted line). The B1-B2 phase boundary is somewhat uncertain beyond the QHA limit of validity of the B2 phase. It is drawn at low pressures only to show the complete comparison of free energies. Dashed and dotted yellow lines are the phase boundaries from *Oganov et al.* [2003] and *Strachan et al.* [1999], respectively.

observed experimentally up to ~2.3 Mbar [*Duffy et al.*, 1995]. Our first principles static calculation indicates that the phase transition from the cubic NaCl-type (B_1 structure), periclase, to CsCl-type structure (B_2) happens at 500GPa, which is in agreement with the previous first principles calculations that predicted 490 GPa [*Oganov et al.*, 2003b], 510 GPa [*Mehl et al.*, 1988; *Jaffe et al.*, 2000; *Habas et al.*, 1998] and 530 GPa [*Umemoto et al.*, 2006]. The QHA phase boundary of the B_1-B_2 transition is depicted in Figure 4. The transition pressure is 490 GPa at 0 K after inclusion of zero point motion and has a negative Clapeyron slope. This can be understood as follows: the number of nearest neighbor changes from six in the B_1 structure to eight in the B_2 structure. This change increases the nearest neighbor distance and decreases vibrational frequencies in overall. The entropy is given by

$$S(V,T) = k_B \sum \left[-\ln(1 - e^{-x_{q,j}}) + k_B \frac{x_{q,j}}{e^{x_{q,j}} - 1} \right] \qquad (7)$$

where $x_{q,j} = \hbar\omega_j\ (q,\ V)/k_BT$, indicates that a decrease in frequency is equivalent to an increase in temperature, i. e., $\Delta S > 0$ for the transition from B_1 to B_2. Then the slope $dP/dT = \Delta S/\Delta V$ is negative since volume decreases during the transition. Figure 4 indicates that our EOS of MgO in the B_1 structure would in principle be a viable pressure standard for experiments conducted even at the highest *PT*s found at the Earth's center.

[11] Table 2 also lists the isochores of MgO derived after the volume and anharmonic corrections are included. From this one can see that both corrections are very small. The anharmonic correction increases with temperature but decreases with volume. It is 0.61 GPa at 3000 K and 74.71 Å^3, the equilibrium volume. A comparison between pressures offered by our corrected EOS and those offered by *Speziale et al.*'s [2001] EOS and *Dorogokupets and Oganov*'s [2007] EOS is offered in Table 3. Thermal pressure in Speziale et al.'s EOS, which was calibrated using the same shock wave data [*Svendsen and Ahrens*, 1987] hence also agrees with the latter, depends on volume. At 0 GPa and 3000 K thermal pressures by these EOSs are very similar, ~17 GPa. At 60% compression and 3000 K, our thermal pressure is ~18.8 GPa, while Speziale et al.'s is ~25.5 GPa. Dorogokupets and Oganov's is more similar to ours, ~19.5 GPa. In general, with increasing pressure, pressure differences between these three scales increase, more so at low temperatures. Speziale et al.'s underestimation of pressure is expected since the internal pressure standard, ruby [*Mao et al.*, 1986], used in their work, has been shown by others [*Dewaele et al.*, 2004; *Chijioke et al.*, 2005; *Aleksandrov et al.*, 1987; *Holzapfel*, 2003; *Kunc et al.*, 2003, 2004; *Dorogokupets and Oganov*, 2007] to underestimate pressure, particularly above 40 GPa. The overestimation of thermal pressure by Speziale et al.'s EOS at ultrahigh pressure leads to considerably larger Clapeyron slope for the $MgSiO_3$ post-

Table 3. Comparison Between Our Corrected EOS With *Speziale et al.*'s [2001] EOS and *Dorogokupets and Oganov*'s [2007] EOS[a]

x = V/V$_o$	300 K	1000 K	2000 K	3000 K
1.0	0.00	4.24	10.68	*17.10*
	(0.00)	(4.32)	(10.98)	*(17.70)*
	[0.00]	[4.17]	[10.35]	*[16.29]*
0.95	9.23	13.45	19.94	*26.43*
	(9.10)	(13.32)	(19.89)	*(26.53)*
	[9.15]	[13.26]	[19.48]	*[25.52]*
0.9	21.31	25.49	32.04	38.60
	(20.83)	(25.10)	(31.78)	(38.54)
	[20.99]	[25.08]	[31.37]	[37.56]
0.85	37.19	41.31	47.92	54.57
	(36.02)	(40.44)	(47.37)	(54.38)
	[36.34]	[40.43]	[46.86]	[53.24]
0.8	58.20	62.26	68.94	75.69
	(55.84)	(60.47)	(67.76)	(75.13)
	[56.30]	[60.41]	[67.03]	[73.65]
0.75	86.20	90.21	96.98	103.86
	(81.93)	(86.84)	(94.57)	(102.39)
	[82.37]	[86.53]	[93.40]	[100.33]
0.7	123.86	127.81	134.71	141.78
	(116.65)	(121.90)	(130.15)	(138.51)
	[116.67]	[120.90]	[128.08]	[135.37]
0.65	175.04	178.94	186.03	193.35
	(163.49)	(169.14)	(178.02)	(187.01)
	[162.18]	[166.50]	[174.06]	[181.79]
0.6	245.51	249.37	256.72	264.35
	(227.72)	(233.83)	(243.45)	(253.18)
	[223.23]	[227.65]	[235.67]	[243.94]

[a]V$_o$ = 74.71 Å^3. Values in parentheses are *Speziale et al.*'s [2001] EOS. Values in brackets are *Dorogokupets and Oganov*'s [2007] EOS. Values in italics are outside the region of validity of our EOS.

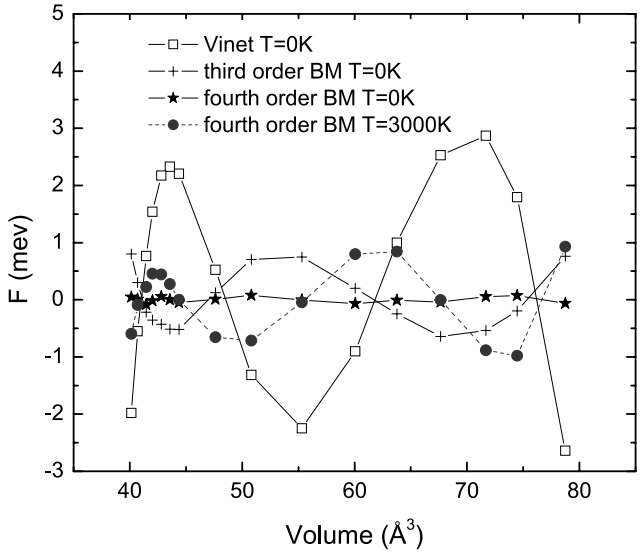

Figure 5. The residual of Helmholtz free energy fits using various fitting functions.

perovskite phase boundary [*Hirose et al.*, 2006; *Ono and Oganov*, 2005] in comparison to other scales.

4. Results and Uncertainties

[12] The numerical calculations and manipulations involved in the "engineering" of these high T EOSs inevitably introduce uncertainties and errors in the predicted pressure. Here we discuss the source and the magnitude of the most significant uncertainties.

[13] First principles calculations have significant uncertainties. But, after combining *any* first principles result with static compression and absolute pressure data at low *PT*s and shock data at high *PT*s this uncertainty is reduced essentially to the experimental uncertainty. At low *PT*s there is a great deal of consistency between various data sets, which reduces the uncertainties to small levels. At shock *PT*s, the Hugoniot equation of state is quite precise. A main source of uncertainty is the shock (Hugoniot) temperature, which is determined by measuring the thermal radiation of shocked MgO at four wavelengths [*Svendsen and Ahrens*, 1987]. A high degree of reproducibility of the shock temperature data indicated that the uncertainty should be within quoted error bars, since shock temperatures obtained by this method were well reproduced by others. For instance, the shock temperature data for iron of *Williams et al.* [1987] are well reproduced by *Yoo et al.* [1993]. The shock temperature data on SiO_2 of *Lyzenga et al.* [1983] were also well reproduced by *Hicks et al.* [2006] using a different method. In addition, the exceptional agreement between first principles results with all shock data points mutually reinforces and validates both results.

[14] Another unavoidable and obvious source of numerical error comes from the choice of the particular EOS: Vinet, third-, or fourth-order Birch-Murnaghan. First principles results are fitted to these EOSs and some fits are better than others. As shown in Figure 5, the residuals of the fits are largest for the Vinet EOS. Third-order Birch-Murnaghan is better but the best fit is obtained with the fourth-order Birch-Murnaghan. The residual sum of squares (RSS) are 2.8×10^{-7} for the Vinet fit, 2.22×10^{-8} for third order, and 2.12×10^{-10} for the fourth order. This conclusion is consistent with *Oganov and Dorogokupets'* [2003] results but contradicts *Cohen et al.*'s [2000] conclusion, which is based on EOSs of metals and molecular solids. Most likely long-range Coulombic (r^{-1}) interactions, which are not explicitly incorporated in the potential function of *Vinet et al.*'s [1989] EOS, are significant in the compression of ionic solids such as MgO. The pressure difference produced by third- and fourth-order EOSs are within 0.2 GPa up to 3 Mbar and then increase to 2 GPa at 5 Mbar. The Vinet EOS pressures differ from the fourth-order EOS pressures 0.5 GPa up to 3 Mbar and then increase to 6 GPa at 5 Mbar. At high temperatures the fitting errors increase even with the fourth order. At 3000 K the RSS is 2.44×10^{-8}. It appears that this should introduce errors comparable to those between the third- and fourth-order at 0 K, i.e., 0.2 GPa up to 3 Mbar and 2 GPa at 5 Mbar.

[15] Hence, we adopt the fourth-order Birch-Murnaghan EOS (equation (2)) with temperature-dependent parameters. The temperature dependence of these parameters are fitted by a fourth-order polynomial in T. After the volume correction described by equation (3) with P_c = 80 GPa, and the empirical anharmonic correction given by equation (6) with c = 0.1, we obtain the coefficients of these polynomial as listed in Table 4. The error introduced by the polynomial fit is less than 0.3% in P up to 5 Mbar. The T dependence of K_0, K'_0, and K''_0 are shown in Figures 6a and 6b. Figure 6a shows very good agreement between our isothermal and adiabatic bulk moduli and those measured by ultrasonic resonance [*Isaak et al.*, 1989] and Brillouin scattering experiments [*Sinogeikin et al.*, 2000] at ambient pressure.

[16] As mentioned above the combination of first principles results with experimental data reduces the uncertainties in the room temperature EOS to the experimental uncertainties. There is however, an intermediate pressure range in which no experimental data is available. In this regime, uncertainties inherent to the first principles part should be estimated. Comparison with all electron calculations offer a sensible estimate of this error. We therefore conducted all electron calculations as similar as possible to our pseudopotential one. These LAPW calculations have been performed using the WIEN2k code [*Blaha et al.*, 2001] and used the same 10 special k points used in pseudopotential calculations. The Muffin-Tin radii (R_{MT}) are chosen to be 1.60 Bohr and 1.55 Bohr for Mg and O, respectively. $R_{MT}^{\min}$ $K_{\max}$ = 8 was used for the expansion of the basis set. The calculation reproduced well previous LAPW results [*Mehl*

Table 4. Coefficients of a Fourth-Order Polynomial Fit of Temperature Dependence of the Equation of State Parameters[a]

	V_0 (Å^3)	K_0 (GPa)	K'_0	A
a_0	74.185	168.80	4.2516	−0.1526
a_1	1.550	−23.22	0.1442	−0.0769
a_2	1.397	−3.573	0.0495	−0.0022
a_3	−0.385	1.107	−0.0195	0.00248
a_4	0.0602	−0.125	0.00404	-6.542×10^{-4}

[a] $Y = a_0 + a_1T + a_2T^2 + a_3T^3 + a_4T^4$. Temperature is in units of 1000 K. Here $A = \frac{3}{8}[K_0K''_0 + (K'_0 - 3)(K'_0 - 4) + 35/9]$.

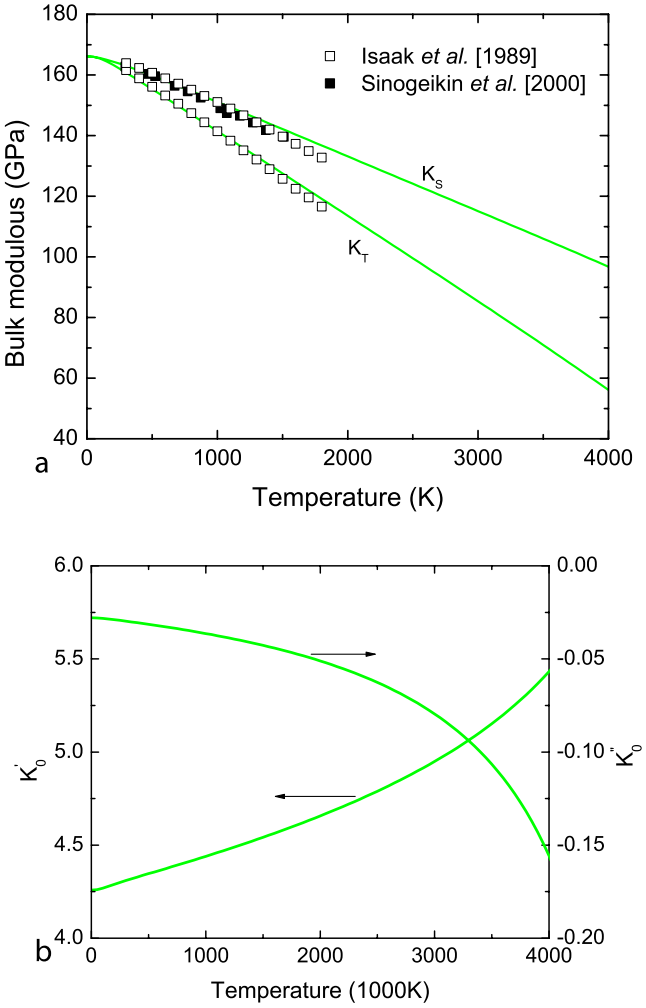

Figure 6. (a) Predicted temperature dependence of isothermal (from K_0 values in Table 4) and adiabatic bulk moduli at zero pressure compared with experiment data, (b) temperature dependence of K'_0 and K''_0 (from K'_0 and A values in Table 4).

et al., 1988]. The LAPW and pseudopotential calculations provide essentially the same K_0 and K'_0, even though the equilibrium volumes differ by about 2.5% (see Table 1 and Figure 7). This difference is not atypical of first principles calculations, but does not compromise the quality of the EOSs offered here. It is possible to bring static pseudopotential and LAPW EOSs, and therefore, LAPW and experimental data into agreement by using a similar correction to that of equation (3): $\Delta V = \Delta V_1 \exp(-P/80) + \Delta V_2$. Static pressures derived from these two calculations differ by less than 1 GPa up to 5 Mbar. Therefore, nearly identical pressure scales could be produced from these two types of calculations. We chose to proceed with our pseudopotential results because they require smaller corrections than LAPW results to match experimental data, including V_o at 300 K and shock data.

[17] The remaining source of uncertainty is the quasi-harmonic calculation that gives the thermal pressure. The accuracy of these calculations for MgO has been extensively documented by comparisons with high T experimental data [*Karki et al.*, 1999; *Karki et al.*, 2000]. Here, we have introduced a correction to account for anharmonic effects which further improves the quality of predictions beyond those of the QHA. After these corrections, thermodynamic properties such as thermal expansivity, α, and bulk modulus, K_T, agree with experimental data within experimental uncertainties (Z. Wu and R. M. Wentzcovitch, manuscript in preparation, 2007) within the region of validity of our EOS (also see Figure 6a). The thermal pressure is given by

$$P_{th} = \int_0^T \alpha K_T dT$$

is approximately linear with temperature, and almost independent of volume. It is about 12 GPa at 2,000 K (11.7 GPa at 0 GPa to 11.4 GPa at 5 Mbar). Therefore, the uncertainty in the thermal pressure should be small. For example, it is less than 0.25 GPa up to 5 Mbar at 2,000 K if the experimental uncertainties in α and K_T are $\sim$1%.

[18] Therefore, we conclude that the combined numerical uncertainties introduced by these factors produce an error approaching 1% in pressure in the entire range of validity of our EOS and is maximum at the highest pressures. However, there are only few shock data points confirming our predicted pressures in the multimegabar regime and this EOS relies heavily on the exceptional agreement of first principles results and shock wave data. Further shock

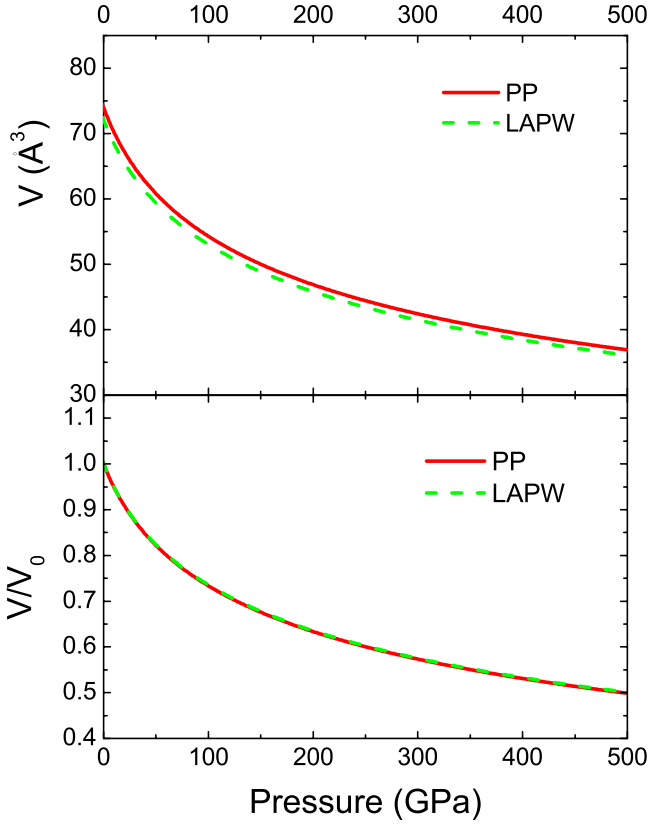

Figure 7. Static EOS from LAPW (dashed line) and pseudopotential (PP) (solid line) calculations.

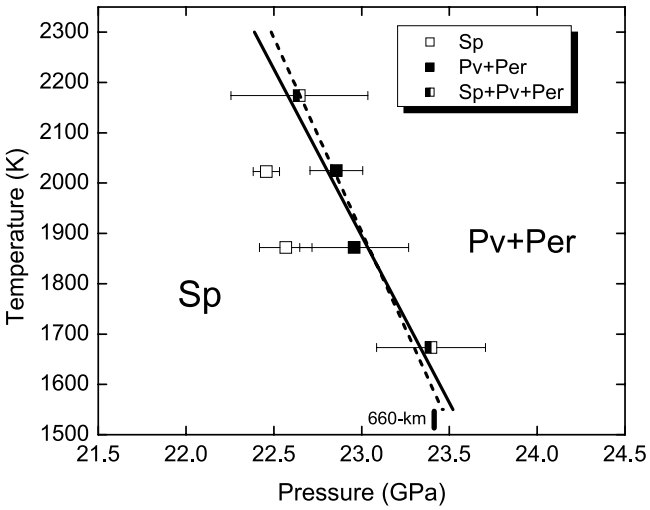

Figure 8. Postspinel phase boundary obtained using our EOS (solid line) and *Speziale et al.*'s [2001] EOS (dashed line).

experiments on MgO are highly desirable for confirmation or further improvements of this EOS.

5. Recalculation of Mantle Phase Transition Boundaries

5.1. Postspinel Phase Transition Boundary

[19] In recent high-pressure experimental studies based on in situ X-ray diffraction measurements, pressures were calculated using high-temperature EOSs of internal pressure standards. However, there is an extensive debate on the accuracy of such EOSs [*Hirose et al.*, 2001; *Fei et al.*, 2004b]. *Irifune et al.* [1998] determined the postspinel phase transition boundary in Mg_2SiO_4 using Au EOS by *Anderson et al.* [1989] as pressure standard. Their results demonstrated that the phase transition occurs at pressures 2.5 GPa lower than that at 660-km depth, i.e., that corresponding to the major seismic discontinuity. Similar experimental study by *Fei et al.* [2004b] used MgO as a pressure standard and the EOSs reported by *Speziale et al.* [2001]. They showed that the transition pressure is very close to that of the 660-km depth and the mismatch is only 0.3 GPa if the temperature is 1873 K at this depth (Figure 8).

[20] Here we recalculated the postspinel phase transition boundary using data by *Fei et al.* [2004b] and our new EOS of MgO (Figure 8). The results show that our EOS predicts very similar pressures to those predicted by *Fei at al.* [2004b] using *Speziale et al.*'s [2001] MgO scale. The former gives transition pressures lager (smaller) by ~0.06 GPa than the latter at 1673 (2173) K. At 660 km depth, i.e., at 23.4 GPa, the transition temperature is ~1580 K and ~1620 K according to *Fei et al.* [2004b], using Speziale et al.'s scale, and by using our EOS, respectively. The Clapeyron slope is −1.3 MPa/K using Speziale et al.'s EOS and −1.5 MPa/K using ours.

5.2. Postperovskite Phase Transition Boundary

[21] *Murakami et al.* [2004] showed that based on the Pt pressure scale proposed by *Jamieson et al.* [1982], the postperovskite phase transition in $MgSiO_3$ [*Murakami et al.*, 2004; *Tsuchiya et al.*, 2004; *Oganov and Ono*, 2004] occurs above 125 GPa and 2500 K. This phase transition boundary was examined later using a different EOS for Pt [*Ono and Oganov*, 2005] and different pressure standards such as Au and MgO [*Hirose et al.*, 2006]. The location of the perovskite to postperovskite phase transition boundary varies by as much as 15 GPa due to inconsistencies between these pressure scales. Moreover, these pressure scales predict significantly different thermal pressures. This leads to large differences in measured Clapeyron slopes, from +5 MPa/K to +11.5 MPa/K [*Ono and Oganov*, 2005; *Hirose et al.*, 2006].

[22] We recalculated the experimental pressures from *Hirose et al.* [2006] based on the present EOS of MgO (Figure 9). Compared to *Speziale et al.*'s [2001] EOS, our EOS gives pressures higher by 3.5 GPa at 1340 K and 2 GPa at 2330 K at 110–120 GPa. The recalculation shows that the postperovskite phase transition in $MgSiO_3$ occurs at 121 GPa, corresponding to 2650-km depth, if the temperature is 2500 K. This matches the location of the D″ seismic discontinuity [e.g., *Wysession et al.*, 1998] at the depths of 2550–2750 km. The Clapeyron slope is estimated to be +9.7 MPa/K, more consistent with results from first principles calculations by *Tsuchiya et al.* [2004] and *Oganov and Ono* [2004] (+7.5 to +10.0 MPa/K) (see Table 5).

[23] Using our present EOS, the postperovskite transition temperature at core-mantle boundary pressures is estimated to be ~3900 K. The double seismic discontinuities within the D″ layer suggests that postperovskite transforms back to perovskite near the base of the mantle due to a strong temperature gradient in the thermal boundary layer [*Thomas et al.*, 2004; *Hernlund et al.*, 2005]. If true, temperatures at the bottom of the mantle should be higher than 3900 K. This is consistent with the estimated value of ~4000 K [*Boehler*, 1996; *Alfè et al.*, 2007] based on the melting temperature of iron at the inner core boundary. Moreover, this temperature

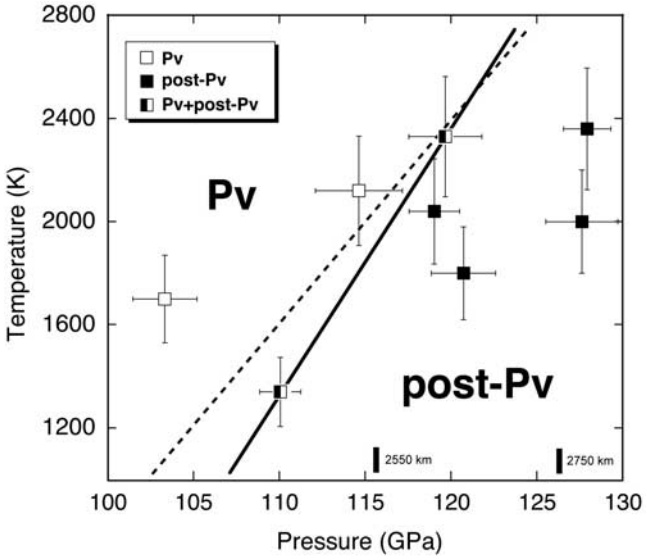

Figure 9. Postperovskite phase boundary obtained using our EOS (solid line) and *Speziale et al.*'s [2001] EOS (dashed line).

Table 5. The Clapeyron Slope of the $MgSiO_3$ Postperovskite Phase Transition

	Clapeyron Slope (MPa/K)	Source
This scale	9.7	*Hirose et al.* [2006]
Speziale et al.'s scale	11.5	*Hirose et al.* [2006]
Tsuchiya et al.'s Au scale	5	*Hirose et al.* [2006]
Holmes et al.'s [1989] Pt scale	7.0	*Ono and Oganov* [2005]
Jamieson et al.'s [1982] Au scale	8.0	*Ono and Oganov* [2005]
Theory	7.5,[a] 9.85[b]	

[a] *Tsuchiya et al.* [2004].
[b] *Oganov and Ono* [2004].

is almost high enough for silicate mantle and subducted MORB crust to melt, which is suggested by a number of seismological observations of ultralow-velocity zone [e.g., *Garnero et al.*, 1998].

6. Summary

[24] In conclusion, our calculated EOS of MgO is in excellent agreement with shock wave data. Therefore, it can be used directly for pressure calibration at pressures P > 100 GPa. At these pressures, our pressures are always larger than those extrapolated from quasi-hydrostatic compression data at lower pressures. Similar conclusion is obtained by comparing the "absolute" pressure calibration by *Li et al.* [2006] with extrapolations of quasi-hydrostatic data. At relatively low *PT*s, our plain first principles EOS requires a volume correction to be useful as pressure calibrant. At low pressures and high temperatures another correction is necessary to account for anharmonic effects and extend the temperature regime of validity of the EOS based on the QHA. Both corrections decrease and eventually vanish with increasing pressure. The validity regime of our EOS, shown in Figure 4, includes the entire *PT* regime of interest to geophysics. The numerical accuracy of this EOS should be close to 1% in its entire range of validity, the error being the largest at the highest pressures, 5 Mbar.

[25] We used this new EOS to recalculate the postspinel and postperovskite phase transition boundaries. Our EOS and *Speziale et al.*'s [2001] are very similar at relatively low pressures. Therefore Clapeyron slope of the postspinel phase transition obtained using either of these scales are very similar too and transition pressure matches well seismic observations. At higher pressures these scales differ considerably. Therefore, the postperovskite phase transition boundary obtained by these scales differ as well. Our EOS gives higher transition pressures at low temperatures which decreases the Clapeyron slope. The new Clapeyron slope of +9.7 MPa/K is more consistent with results of first principles calculations (+7.5 to +10.0 MPa/K) [*Tsuchiya et al.*, 2004; *Oganov and Ono*, 2004]. The postperovskite phase boundary obtained with our EOSs matches the location of the D″ seismic discontinuity and supports the idea that postperovskite transforms back to perovskite before the core-mantle boundary.

[26] **Acknowledgments.** We thank Thomas Ahrens for useful discussions on the shock compressed data. Calculations were performed at the Minnesota Supercomputing Institute (MSI) with the Quantum ESPRESSO package (http://www.pwscf.org). Work was supported by NSF/EAR 0230319, 0635990, and NSF/ITR 0428774 (VLab).

References

Akahama, Y., H. Kawamura, and A. K. Singh (2002), Equation of state of bismuth to 222 GPa and comparison of gold and platinum pressure to 145 GPa, *J. Appl. Phys.*, *92*, 5892–5897, doi:10.1063/1.1515378.

Aleksandrov, I. V., A. F. Goncharov, A. N. Zisman, and A. M. Stishov (1987), Diamond at high pressures—Raman scattering of light, equation of state, and a high pressure scale, *Sov. Phys. JETP*, Engl. Transl., *66*, 384–390.

Alfè, D. (2005), Melting curve of MgO from first-principles simulations, *Phys. Rev. Lett.*, *94*, 235701, doi:10.1103/PhysRevLett.94.235701.

Alfè, D., M. Alfredsson, J. Brodholt, M. J. Gillan, M. D. Towler, and R. J. Needs (2005), Quantum Monte Carlo calculations of the structural properties and the B1–B2 phase transition of MgO, *Phys. Rev. B*, *72*, 014114, doi:10.1103/PhysRevB.72.014114.

Alfè, D., M. J. Gillan, and G. D. Price (2007), Temperature and composition of the Earth's, *Contemp. Phys.*, *48*, 63–80, doi:10.1080/00107510701529653.

Anderson, O. L. (1997), The volume dependence of thermal pressure in solids, *J. Phys. Chem. Solids*, *58*, 335–343.

Anderson, O. L., D. G. Isaak, and S. Yamamoto (1989), Anharmonicity and the equation of state for gold, *J. Appl. Phys.*, *65*, 1534–1543, doi:10.1063/1.342969.

Baroni, S., S. de Gironcoli, A. Dal Corso, and P. Giannozzi (2001), Phonons and related crystal properties from density-functional perturbation theory, *Rev. Mod. Phys.*, *73*, 515–562, doi:10.1103/RevModPhys.73.515.

Belonoshko, A. B., and L. S. Dubrovinsky (1996), Molecular dynamics of NaCl (B1 and B2) and MgO (B1) melting; two-phase simulation, *Am. Mineral.*, *81*, 303–316.

Blaha, P., K. Schwarz, G. K. H. Madsen, D. Kvasnicka, and J. Luitz (2001), *WIEN2k, An Augmented Plane Wave + Local Orbitals Program for Calculating Crystal Properties*, edited by K. Schwarz, Vienna Univ. of Technol, Vienna, Austria.

Boehler, R. (1996), Melting temperature of the Earth's mantle and core: Earth's thermal structure, *Annu. Rev. Earth Planet. Sci.*, *24*, 15–40.

Carrier, P., R. Wentzcovitch, and J. Tsuchiya (2007), First-principles prediction of crystal structures at high temperatures using the quasi-harmonic approximation, *Phys. Rev. B*, *76*, 064116, doi:10.1103/PhysRevB.76.064116.

Ceperley, D. M., and B. J. Alder (1980), Ground state of the electron gas by a stochastic method, *Phys. Rev. Lett.*, *45*, 566–569, doi:10.1103/PhysRevLett.45.566.

Chijioke, A. D., W. J. Nellis, and I. F. Silvera (2005), High-pressure equations of state of Al, Cu, Ta, and W, *J. Appl. Phys.*, *98*, 073526, doi:10.1063/1.2071449.

Cohen, R. D., O. Gulseren, and R. J. Henley (2000), Accuracy of equation-of-state formulations, *Am. Mineral.*, *85*, 338–344.

Cohen, R. E., and Z. Gong (1994), Melting and melt structure of MgO at high pressures, *Phys. Rev. B*, *50*, 12,301–12,311, doi:10.1103/PhysRevB.50.12301.

Dal Corso, A., S. Baroni, R. Resta, and S. de Gironcoli (1993), Ab initio calculation of phonon dispersions in II–VI semiconductors, *Phys. Rev. B*, *47*, 3588–3592.

Dewaele, A., G. Fiquet, D. Andrault, and D. Hausermann (2000), P-V-T equation of state of periclase from synchrotron radiation measurements, *J. Geophys. Res.*, *105*, 2869–2877, doi:10.1029/1999JB900364.

Dewaele, A., P. Loubeyre, and M. Mezouar (2004), Equations of state of six metals above 94 GPa, *Phys. Rev. B*, *70*, 094112, doi:10.1103/PhysRevB.70.094112.

Dorogokupets, P. I., and A. R. Oganov (2007), Ruby, metals, and MgO as alternative pressure scales: A semiempirical description of shockwave, ultrasonic, X-ray, and thermochemical data at high temperatures and pressures, *Phys. Rev. B*, *75*, 024115, doi:10.1103/PhysRevB.75.024115.

Dubrovinsky, L., et al. (2003), Iron-silica interaction at extreme conditions and the electrically conducting layer at the base of Earth's mantle, *Nature*, *422*, 58–61, doi:10.1038/nature01422.

Duffy, T. S., R. J. Hemley, and H.-K. Mao (1995), Equation of state and shear strength at multimegabar pressures: Magnesium oxide to 227 GPa, *Phys. Rev. Lett.*, *74*, 1371–1374, doi:10.1103/PhysRevLett.74.1371.

Fei, Y. (1999), Effects of temperature and composition on the bulk modulus of (Mg,Fe)O, *Am. Mineral.*, *84*, 272–276.

Fei, Y., L. Jie, K. Hirose, W. Minarik, J. V. Orman, C. Sanloup, W. Westrenen, T. Komabayashi, and K. Funakoshi (2004a), A critical evaluation of pressure scales at high temperatures by in situ X-ray diffraction

measurements, *Phys Earth Planet Inter*, *143–144*, 515–526, doi:10.1016/j.pepi.2003.09.018.

Fei, Y., J. V. Orman, J. Li, W. V. Westrenen, C. Sanloup, W. Minarik, K. Hirose, T. Komabayashi, M. Walter, and K. Funakoshi (2004b), Experimentally determined postspinel transformation boundary in Mg_2SiO_4 using MgO as an internal pressure standard and its geophysical implications, *J. Geophys. Res.*, *109*, B02305, doi:10.1029/2003JB002562.

Fei, Y., A. Ricolleau, M. Frank, K. Mibe, G. Shen, and V. Prakapenka (2007), Toward an internally consistent pressure scale, *Proc. Natl. Acad. Sci. U. S. A.*, *104*, 9182–9186, doi:10.1073/pnas.0609013104.

Fiquet, G., P. Richet, and G. Montagnac (1999), High-temperature thermal expansion of lime, periclase, corundum and spinel, *Phys. Chem. Miner.*, *27*, 103–111, doi:10.1007/s002690050246.

Garnero, E., J. Revenaugh, Q. Williams, T. Lay, and L. Kellog (1998), Ultralow velocity zone at the core-mantle boundary, in *The Core-Mantle Boundary Region*, *Geodyn. Ser.*, vol. 28, edited by M. Gurnis et al., pp. 319–334, AGU, Washington, D. C.

Habas, M.-P., R. Dovesi, and A. Lichanot (1998), The B_1, B_2 phase transition in alkaline-earth oxides: a comparison of ab initio Hartree-Fock and density functional calculations, *J. Phys. Condens. Matter*, *10*, 6897–6909, doi:10.1088/0953-8984/10/31/008.

Hernlund, J. W., C. Thomas, and P. J. Tackley (2005), A doubling of the post-perovskite phase boundary and structure of the Earth's lowermost mantle, *Nature*, *434*, 882–886, doi:10.1038/nature03472.

Hicks, D. G., T. R. Boehly, J. H. Eggert, J. E. Miller, P. M. Celliers, and G. W. Collins (2006), Dissociation of liquid silica at high pressures and temperatures, *Phys. Rev. Lett.*, *97*, 025502, doi:10.1103/PhysRevLett.97.025502.

Hirose, K., T. Komabayashi, M. Murakami, and K. Funakoshi (2001), In-situ measurements of the majorite-akimotoite-perovskite phase transition boundaries in $MgSiO_3$, *Geophys. Res. Lett.*, *28*, 4351–4354, doi:10.1029/2001GL013549.

Hirose, K., R. Sinmyo, N. Sata, and Y. Ohishi (2006), Determination of post-perovskite phase transition boundary in MgSiO3 using Au and MgO internal pressure standards, *Geophys. Res. Lett.*, *33*, L01310, doi:10.1029/2005GL024468.

Holmes, N., J. Moriarty, G. Gather, and W. Nellis (1989), The equation of state of platinum to 660 GPa (6.6 Mbar), *J. Appl. Phys.*, *66*, 2962–2967, doi:10.1063/1.344177.

Holzapfel, W. B. (2003), Refinement of the ruby luminescence pressure scale, *J. Appl. Phys.*, *93*, 1813–1818, doi:10.1063/1.1525856.

Inbar, I., and R. E. Cohen (1995), High pressure effects on thermal properties of MgO, *Geophys. Res. Lett.*, *22*, 1533–1536, doi:10.1029/95GL01086.

Irifune, T., et al. (1998), The post-spinel phase boundary in Mg_2SiO_4 determined by in-situ X-ray diffraction, *Science*, *279*, 1698–1700, doi:10.1126/science.279.5357.1698.

Isaak, D. G., O. L. Anderson, and T. Goto (1989), Measured elastic moduli of single-crystal MgO up to 1800 K, *Phys. Chem. Miner.*, *16*, 704–713, doi:10.1007/BF00223321.

Isshiki, M., T. Irifune, K. Hirose, S. Ono, Y. Ohishi, T. Watanuki, E. Nishibori, M. Takata, and M. Sakata (2004), Stability of magnesite and its high-pressure form in the lowermost mantle, *Nature*, *427*, 60–63, doi:10.1038/nature02181.

Jackson, I., and H. Neisler (1982), The elasticity of periclase to 3 GPa and some geophysical implications, in *High-pressure Research: Application to Earth and Planetary Sciences*, *Geophys. Monogr. Ser*, vol. 67, edited by S. Akimoto and M. H. Manghnani, pp. 93–113, Terra Sci, Tokyo.

Jaffe, J. E., J. A. Snyder, Z. Lin, and A. C. Hess (2000), LDA and GGA calculations for high-pressure phase transitions in ZnO and MgO, *Phys. Rev. B*, *62*, 1660–1665, doi:10.1103/PhysRevB.62.1660.

Jamieson, J. C., J. N. Fritz, and M. H. Manghnani (1982), Pressure measurement at high temperature in x-ray diffraction studies: Gold as a primary standard, in *High-Pressure Research: Application to Earth and Planetary Sciences*, *Geophys. Monogr. Ser.*, vol. 67, edited by S. Akimoto and M. H. Manghnani, pp. 27–48, Terra Sci., Tokyo.

Karki, B. B. (2000), Thermal pressure in MgO and $MgSiO_3$ perovskite at lower mantle conditions, *Am. Mineral.*, *85*, 1447–1451.

Karki, B. B., R. M. Wentzcovitch, S. de Gironcoli, and S. Baroni (1999), First-principles determination of elastic anisotropy and wave velocities of MgO at lower mantle conditions, *Science*, *286*, 1705–1707, doi:10.1126/science.286.5445.1705.

Karki, B. B., R. M. Wentzcovitch, S. De Gironcoli, and S. Baroni (2000), High-pressure lattice dynamics and thermoelasticity of MgO, *Phys. Rev. B*, *61*, 8793–8800, doi:10.1103/PhysRevB.61.8793.

Kunc, K., I. Loa, and K. Syassen (2003), Equation of state and phonon frequency calculations of diamond at high pressures, *Phys. Rev. B*, *68*, 094107, doi:10.1103/PhysRevB.68.094107.

Kunc, K., I. Loa, and K. Syassen (2004), Diamond under pressure: Ab-initio calculations of the equation of state and optical phonon frequency revisited, *High Pressure Res.*, *24*, 101–110, doi:10.1080/08957950310001635765.

Li, B., K. Woody, and J. Kung (2006), Elasticity of MgO to 11 GPa with an independent absolute pressure scale: Implications for pressure calibration, *J. Geophys. Res.*, *111*, B11206, doi:10.1029/2005JB004251.

Loubeyre, P., F. Occelli, and R. LeToullec (2002), Optical studies of solid hydrogen to 320 GPa and evidence for black hydrogen, *Nature*, *416*, 613–617, doi:10.1038/416613a.

Lu, L. Y., Y. Cheng, X. R. Chen, and J. Zhu (2005), Thermodynamic properties of MgO under high pressure from first-principles calculations, *Physica B*, *370*, 236–242, doi:10.1016/j.physb.2005.09.017.

Lyzenga, G. A., T. J. Ahrens, and A. C. Mitchell (1983), Shock temperatures of SiO_2 and their implications, *J. Geophys. Res.*, *88*, 2431–2444.

Mao, H. K., J. Xu, and P. M. Bell (1986), Calibration of the ruby pressure gauge to 800 kbar under quasi-hydrostatic conditions, *J. Geophys. Res.*, *91*, 4673–4676, doi:10.1029/JB091iB05p04673.

Matsui, M., S. C. Parker, and M. Leslie (2000), The MD simulation of the equation of state of MgO: Application as a pressure calibration standard at high temperature and high pressure, *Am. Mineral.*, *85*, 312–316.

Mehl, M. J., R. E. Cohen, and H. Krakauer (1988), Linearized augmented plane wave electronic structure calculations for MgO and CaO, *J. Geophys. Res.*, *93*, 8009–8022, doi:10.1029/JB093iB07p08009.

Murakami, M., K. Hirose, K. Kawamura, N. Sata, and Y. Ohishi (2004), Post-perovskite phase transition in $MgSiO_3$, *Science*, *304*, 855–858, doi:10.1126/science.1095932.

Oganov, A. R., and P. I. Dorogokupets (2003), All-electron and pseudopotential study of MgO: Equation of state, anharmonicity, and stability, *Phys. Rev. B*, *67*, 224110, doi:10.1103/PhysRevB.67.224110.

Oganov, A. R., and S. Ono (2004), Theoretical and experimental evidence for a post-perovskite phase of $MgSiO_3$ in Earth's D'' layer, *Nature*, *430*, 445–448, doi:10.1038/nature02701.

Oganov, A. R., M. J. Gillan, and G. D. Price (2003), Ab initio lattice dynamics and structural stability of MgO, *J. Chem. Phys.*, *118*, 10,174–10,182, doi:10.1063/1.1570394.

Ono, S., and A. R. Oganov (2005), In situ observations of phase transition between perovskite and $CaIrO_3$-type phase in $MgSiO_3$ and pyrolitic mantle composition, *Earth Planet. Sci. Lett.*, *236*, 914–932, doi:10.1016/j.epsl.2005.06.001.

Perdew, J. P., and A. Zunger (1981), Self-interaction correction to density-functional approximations for many-electron systems, *Phys. Rev. B*, *23*, 5048–5079, doi:10.1103/PhysRevB.23.5048.

Ruoff, A. L., R. C. Lincoln, and Y. C. Chen (1973), A new method of absolute high pressure determination, *J. Phys. D Appl. Phys.*, *6*, 1295–1306, doi:10.1088/0022-3727/6/10/315.

Sinogeikin, S. V., J. M. Jackson, B. O'Neill, J. W. Palko, and J. D. Bass (2000), Compact high-temperature cell for Brillouin scattering measurements, *Rev. Sci. Instrum.*, *71*, 201–206, doi:10.1063/1.1150183.

Speziale, S., C. Zha, T. S. Duffy, R. J. Hemley, and H. K. Mao (2001), Quasi-hydrostatic compression of magnesium oxide to 52 GPa: implications for the pressure-volume-temperature equation of state, *J. Geophys. Res.*, *106*, 515–528, doi:10.1029/2000JB900318.

Strachan, A., T. Çagin, and W. A. Goddard III (1999), Phase diagram of MgO from density-functional theory and molecular-dynamics simulations, *Phys. Rev. B*, *60*, 15,084–15,093, doi:10.1103/PhysRevB.60.15084.

Svendsen, B., and T. J. Ahrens (1987), Shock-induced temperatures of MgO, *Geophys. J. R. Astron. Soc.*, *91*, 667–691.

Thomas, C., E. J. Garnero, and T. Lay (2004), High-resolution imaging of lowermost mantle structure under the Cocos plate, *J. Geophys. Res.*, *109*, B08307, doi:10.1029/2004JB003013.

Troullier, N., and J. L. Martins (1991), Efficient pseudopotentials for plane-wave calculations, *Phys. Rev. B*, *43*, 1993–2006, doi:10.1103/PhysRevB.43.1993.

Tsuchiya, T., J. Tsuchiya, K. Umemoto, and R. M. Wentzcovitch (2004), Phase transition in $MgSiO_3$ perovskite in the Earth's lower mantle, *Earth Planet. Sci. Lett.*, *224*, 241–248, doi:10.1016/j.epsl.2004.05.017.

Umemoto, K., R. M. Wentzcovitch, and P. B. Allen (2006), Dissociation of $MgSiO_3$ in the cores of gas giants and terrestrial exoplanets, *Science*, *311*, 983–986, doi:10.1126/science.1120865.

Utsumi, W., D. J. Weidner, and R. C. Lieberman (1998), Volume measurement of MgO at high pressures and high temperatures, in *Properties of Earth and Planetary Materials at High Pressure and Temperature*, *Geophys. Monogr. Ser.*, vol. 101, edited by M. H. Manghnani and T. Yagi, pp. 327–333, AGU, Washington, D. C.

Vassiliou, M. S., and T. J. Ahrens (1981), Hugoniot equation of state of periclase to 200 GPa, *Geophys. Res. Lett.*, *8*, 729–732, doi:10.1029/GL008i007p00729.

Vinet, P., J. H. Rose, J. Ferrante, and J. R. Smith (1989), Universal features of the equation of state of solids, *J. Phys. Condens. Matter*, *1*, 1941–1963, doi:10.1088/0953-8984/1/11/002.

Vočadlo, L., and G. D. Price (1996), The melting of MgO—Computer calculations via molecular dynamics, *Phys. Chem. Miner.*, *23*, 42–49, doi:10.1007/BF00202992.

Wallace, D. (1972), *Thermodynamics of Crystals*, John Wiley, New York.

Wentzcovitch, R. M., B. B. Karki, M. Cococcioni, and S. de Gironcoli (2004), Thermoelastic properties of $MgSiO_3$-perovskite: Insights on the nature of the Earth's lower mantle, *Phys. Rev. Lett.*, *92*, 018501.

Williams, Q., R. Jeanloz, J. Bass, B. Svendsen, and T. J. Ahrens (1987), The melting curve of iron to 250 gigapascals: a constraint on the temperature at Earth's center, *Science*, *236*, 181–182, doi:10.1126/science.236.4798.181.

Wysession, M. E., T. Lay, J. Revenaugh, Q. Williams, E. J. Garnero, R. Jeanloz, and L. H. Kellogg (1998), The D″ discontinuity and its implications, in *The Core-Mantle Boundary Region*, *Geodyn. Ser.*, vol. 28, edited by M. Gurnis et al., pp. 273–297, AGU, Washington, D. C.

Yoo, C. S., N. C. Holmes, M. Ross, D. G. Webb, and C. Pike (1993), Shock temperatures and melting of iron at Earth core conditions, *Phys. Rev. Lett.*, *70*, 3931–3934, doi:10.1103/PhysRevLett.70.3931.

Zerr, A., and R. Boehler (1994), Constraints on the melting temperature of the lower mantle from high-pressure experiments on MgO and magnesiowüstite, *Nature*, *371*, 506–508, doi:10.1038/371506a0.

Zha, C., H. Mao, and R. J. Hemley (2000), Elasticity of MgO and a primary pressure scale to 55 GPa, *Proc. Natl. Acad. Sci. U. S. A.*, *97*, 13,494–13,499, doi:10.1073/pnas.240466697.

Zhang, H., and M. S. T. Bukowinski (1991), Modified potential-induced-breathing model of potentials between close-shell ions, *Phys. Rev. B*, *44*, 2495–2503, doi:10.1103/PhysRevB.44.2495.

K. Hirose, Department of Earth and Planetary Sciences, Tokyo Institute of Technology, 2-12-1 Ookayama, Meguro, Tokyo, 152-8551, Japan.

B. Li, Mineral Physics Institute, State University of New York at Stony Brook, Stony Brook, NY 11794, USA.

K. Umemoto, R. M. Wentzcovitch, and Z. Wu, Department of Chemical Engineering and Materials Science, University of Minnesota Twin Cities, Minneapolis, MN 55455, USA. (wuzq@cems.umn.edu)

J.-C. Zheng, Condensed Matter Physics and Materials Science Department, Brookhaven National Laboratory, P.O. Box 5000, Upton, NY 11973-5000, USA.